J Biomol NMR (2012) 52:339–350
DOI 10.1007/s10858-012-9614-9

ARTICLE

NMR analysis of Lys63-linked polyubiquitin recognition by the tandem ubiquitin-interacting motifs of Rap80

Naotaka Sekiyama · JunGoo Jee · Shin Isogai · Ken-ichi Akagi · Tai-huang Huang · Mariko Ariyoshi · Hidehito Tochio · Masahiro Shirakawa

Received: 16 December 2011 / Accepted: 31 January 2012 / Published online: 18 February 2012

Abstract Ubiquitin is a post-translational modifier that is involved in cellular functions through its covalent attachment to target proteins. Ubiquitin can also be conjugated to itself at seven lysine residues and at its amino terminus to form eight linkage-specific polyubiquitin chains for individual cellular processes. The Lys63-linked polyubiquitin chain is recognized by tandem ubiquitin-interacting motifs (tUIMs) of Rap80 for the regulation of DNA repair. To understand the recognition mechanism between the Lys63-linked diubiquitin (K63-Ub_2) and the tUIMs in solution, we determined the solution structure of the K63-Ub_2:tUIMs complex by using NOE restraints and RDC data derived from NMR spectroscopy. The structure showed that the tUIMs adopts a nearly straight and single continuous α-helix, and the two ubiquitin units of the K63-Ub_2 separately bind to each UIM motif. The interfaces are formed between Ile44-centered patches of the two ubiquitin units and the hydrophobic residues of the tUIMs. We also showed that the linker region between the two UIM motifs possesses a random-coil conformation in the free state, but undergoes the coil-to-helix transition upon complex formation, which simultaneously fixes the relative position of ubiquitin subunits. These data suggest that the relative position of ubiquitin subunits in the K63-Ub_2:tUIMs complex is essential for linkage-specific binding of Rap80 tUIMs.

The atomic coordinates of the K63-Ub_2:$tUIM_{Rap80}$ complex structure have been deposited in the Protein Data Bank under PDB ID code 2RR9.

Electronic supplementary material The online version of this article (doi:10.1007/s10858-012-9614-9) contains supplementary material, which is available to authorized users.

N. Sekiyama · S. Isogai · M. Ariyoshi · H. Tochio (✉) · M. Shirakawa (✉)
Graduate School of Engineering, Kyoto University, Kyoto daigaku-Katsura, Nishikyo-ku, Kyoto 615-8510, Japan
e-mail: tochio@moleng.kyoto-u.ac.jp

M. Shirakawa
e-mail: shirakawa@moleng.kyoto-u.ac.jp

J. Jee
Center for Priority Areas, Tokyo Metropolitan University, 1-1 Minami-Osawa, Hachioji, Tokyo 192-0397, Japan

K. Akagi
Section of Laboratory Equipments, National Institute of Biomedical Innovation, 7-6-8, Asagi, Saito, Ibaraki, Osaka 567-0085, Japan

T. Huang
Division of Structural Biology, Institute of Biomedical Sciences, Academia Sinica, Nankang, Taipei 11529, Taiwan

Present Address:
M. Ariyoshi
Institute for Integrated Cell-Material Sciences (iCeMS), Kyoto University, Yoshida Ushinomiya-cho, Sakyo-ku, Kyoto 606-8501, Japan

M. Ariyoshi
Japan Science and Technology PRESTO, 4-1-8 Honcho Kawaguchi, Saitama 332-0012, Japan

M. Shirakawa
CREST, Japan Science and Technology Corporation, Kawaguchi, Saitama 332-0012, Japan

M. Shirakawa
Genome Science Center, RIKEN, Tsurumi, Yokohama 230-0045, Japan

Keywords Ubiquitin · Lys63-linked polyubiquitin chains · Rap80 · Tandem ubiquitin-interacting motifs · NMR spectroscopy

Introduction

Ubiquitin (Ub), a conserved 76-amino-acid protein, regulates diverse cellular functions through its conjugation to substrate proteins (Hicke 2001). The covalent attachment of ubiquitin to target proteins is carried out via sequential enzymatic pathways that catalyze the formation of an isopeptide bond between the carboxyl terminus (C-terminal) glycine residue of ubiquitin and the ε-amino group of a lysine residue of the target protein (Hershko and Ciechanover 1998). This isopeptide bond can also be formed between two or more ubiquitin molecules, resulting in polyubiquitin chains (polyUb) (Pickart and Fushman 2004). All eight amino groups of ubiquitin, comprising seven lysine residues (Lys6, Lys11, Lys27, Lys29, Lys33, Lys48 and Lys63) and the amino terminus, can be linked to the C-terminus of another molecule, allowing the formation of eight polyUb linkage types. Some of these linkage-specific polyUb have been implicated in specific cellular functions, such as protein degradation, immune signaling and DNA repair (Ikeda and Dikic 2008).

The linkage-specific functions of polyUb are attributed to their structural properties; the crystal structure of Lys48-linked tetraubiquitin has a compact conformation (Eddins et al. 2007), whereas crystallographic and NMR analyses suggest substantial flexibility in the unit junction in Lys63-linked polyUb (Varadan et al. 2004). These higher-order polyUb structures are recognized by effectors containing ubiquitin-binding domains (UBDs) (Hicke et al. 2005). To date, the crystal structures of complexes of the linear (Rahighi et al. 2009), Lys48- (Zhang et al. 2009) or Lys63-linked (Kulathu et al. 2009; Newton et al. 2008; Sato et al. 2009a, b) diubiquitin chains and UBDs have revealed the molecular mechanisms underlying the linkage-specific recognition of diubiquitin; the UBDs principally contact hydrophobic patches centered on Ile44 of the two ubiquitins, which have fixed relative positions in the crystal structures but do not interact with the isopeptide bond, except for a ubiquitin isopeptidase AMSH that directly recognizes the isopeptide bond of Lys63-linked diubiquitin (Sato et al. 2008).

Lys63-linked polyUb is specifically recognized by the tandem ubiquitin-interacting motifs (tUIM) of Rap80, which play a key role in DNA damage repair (Kim et al. 2007; Sobhian et al. 2007). The recently reported crystal structure of the mouse Rap80 tUIM in complex with Lys63-linked diubiquitin (K63-Ub_2) shows that the tUIM adopt a long persistent α-helix (Sato et al. 2009a) while circular dichroism measurements suggest that a random-coil to helix transition is induced in the linker region of the tUIM upon complex formation (Sims and Cohen 2009). This structural feature is unique to the tUIM compared to other tandem UBD domains such as tandem UIM motifs in Vps27 and S5a or tandem UBA domains of hHR23a, which are linked through a flexible linker (Swanson et al. 2003; Wang et al. 2003; Wang et al. 2005). More recently, NMR analyses in combination with molecular dynamics simulations of the Rap80 tUIM have revealed that the tUIM are in equilibrium between random-coil and helical states in the free state and that the linker region between the two motifs retains flexibility even in complex with linear polyUb (Markin et al. 2010). The inherent flexibility exhibited by both the Rap80 tUIM and K63-Ub_2 in the free solution state raises a possibility that the crystal structure of the complex between the tUIM and K63-Ub_2 was somewhat affected by crystal packing forces. Therefore, the solution structure of the complex needs to be examined.

Herein we report a solution structure of Rap80 tUIM in a complex with the K63-Ub_2. Paramagnetic relaxation enhancement (PRE) experiments unambiguously define the relative orientation of the tUIM to K63-Ub_2 in solution state. The conventional NMR method for determining multiprotein complexes relies on short-range distance information derived from nuclear Overhauser effects (NOEs), which is generally insufficient for defining the structure that contains a flexible linker between two domains because such a region usually suffers from a low density of NOE- derived distance restraints. We therefore employed residual dipolar coupling (RDC) constants as long-range structure restraints to supplement NOE restraints. The result indicated that the complex structure in solution is essentially identical to the crystal structure. The $\{^1H\}$-^{15}N hetero NOE experiments revealed that the inter UIM linker and the two UIM motifs gain substantial rigidity upon complex formation, which aligns two UIM helices in the long persistence helix and simultaneously arranges the relative position of the ubiquitin subunits in an optimal position for binding.

Materials and methods

Sample preparation of the Rap80 tandem UIMs

A cDNA fragment (138 base pairs) encoding the tUIM of human Rap80 (residues 79-124) was synthesized by polymerase chain reaction using six 50-mer DNA oligonucleotides as previously described (Ito and Wagner 2004), and the fragment was subcloned into the pET-28a *Escherichia coli* (*E. coli*) expression vector (Novagen), which was engineered for protein expression with N-terminal

hexahistidine (His6) and small ubiquitin-like modifier-3 (SUMO-3) fusion tags.

Escherichia coli strain BL21(DE3) cells expressing the tUIM were grown in H_2O or 70% D_2O minimal medium containing $^{15}NH_4Cl$ and $^{13}C_6$-D-glucose as the sole nitrogen and carbon sources, respectively. *E. coli* cells expressing the unlabeled tUIM were grown in LB medium. Cells were grown at 37°C until the bacterial optical density at 660 nm reached 0.4 and were then induced with 0.5 mM isopropyl β-D-1-thiogalactopyranoside (IPTG). After incubation at 25°C for 12 h, the cells were harvested, resuspended in lysis buffer (50 mM Tris–HCl, pH 7.5, 500 mM NaCl, 10 mM imidazole, 5 mM 2-mercaptoethanol and 0.1 mM phenylmethylsulphonyl fluoride (PMSF)) and disrupted by sonication at 4°C. After centrifugation, the supernatant was applied to a metal-affinity column (Ni–NTA; Qiagen) equilibrated with PMSF-free lysis buffer, and the His6-SUMO-3 fusion protein was eluted with elution buffer (50 mM Tris–HCl, pH 7.5, 500 mM NaCl, 200 mM imidazole and 5 mM 2-mercaptoethanol). The His6-SUMO-3 tag was then removed by digestion with the SUMO-specific protease GST-SENP2 for 12 h at 4°C. After dialysis against a buffer of 50 mM Tris–HCl, pH 7.5, 500 mM NaCl, 10 mM imidazole and 5 mM 2-mercaptoethanol, the sample was loaded onto the metal-affinity column to remove the His6-SUMO-3 tag. The protein solution was further purified using a size-exclusion HiLoad 16/60 Superdex 75 column (GE Healthcare Bio-Sciences) equilibrated with 50 mM Tris–HCl, pH 7.5, 500 mM NaCl and 1 mM DTT.

Preparation of K63-Ub_2 and the K63-Ub_2:tUIM complex

Wild-type and mutant (D77, K63C and K48C) ubiquitin constructs were prepared as previously reported (Tenno et al. 2004). The Lys48-link-specific E2 enzyme, E2-25 K, and the yeast Lys63-link-specific E2 enzyme, Mms2-Ubc13, were expressed in *E. coli* and purified. The E1 enzyme was expressed in Sf9 insect cells and purified as described (Tenno et al. 2004). To prepare Lys63-linked diubiquitin (K63-Ub_2), we used the ubiquitin derivatives D77 (Ub-D77) and K63C (Ub-K63C); D77 contains an additional aspartic acid at its C-terminus while Ub-K63C has a single lysine-to-cysteine mutation at position 63. These two ubiquitin mutants enable the enzymatic synthesis of K63-Ub_2, which is composed of Ub-D77 and Ub-K63C at the proximal and distal positions, respectively. An isotope label was induced selectively to the proximal Ub-D77 in K63-Ub_2 by incubating labeled Ub-D77 and unlabeled Ub-K63C with 0.1 μM E1, 4 μM E2 and 4 mM ATP at 37°C for 12 h. K63-Ub_2 specifically labeled at the distal Ub-K63C was prepared in the reciprocal manner and purified on an ion-exchange Q Sepharose FF column (GE Healthcare Bio-Sciences) and a size-exclusion Hiload 16/60 Superdex 75 column (GE Healthcare Bio-Sciences) equilibrated with 50 mM Tris–HCl, pH 7.5, 150 mM NaCl and 1 mM DTT. The Lys48-linked diubiquitin (K48-Ub_2) was prepared using Ub-D77 and the K48C ubiquitin (Ub-48C) mutants. K63-Ub_2 was incubated with a 1.5-fold molar excess of the tUIM to form the complex. The stoichiometric complex of K63-Ub_2 with the tUIM was purified using a size-exclusion Hiload 16/60 Superdex 75 column (GE Healthcare Bio-Sciences) equilibrated with 50 mM Tris–HCl, pH 7.5, 150 mM NaCl and 1 mM DTT.

NMR measurements

All NMR experiments were performed at 310 K on a Bruker Avance-600, Avance-700 or Avance II-800 spectrometer. Data processing and analysis were performed using NMRPipe (Delaglio et al. 1995) and Sparky (Goddard and Kneller), respectively.

Sequential backbone chemical shift assignments of the free and complexed tUIM were obtained from the following experiments: 2D ^{1}H-^{15}N HSQC, 3D HNCO, 3D CBCA(-CO)NH, 3D HNCACB and 3D ^{1}H-^{13}C HSQC-NOESY-^{1}H-^{15}N HSQC (Diercks et al. 1999) recorded on 2.0 mM [^{15}N,^{13}C]-labeled free tUIM or 2.4 mM [^{15}N,^{13}C]-labeled tUIM in complex with non-labeled K63-Ub_2 complex. The side chain chemical shifts of the tUIM in the complex were assigned using three spectra: 3D CC(CO)NH, 3D HCC(CO)NH and 2D ^{1}H-^{13}C HSQC recorded on 2.0 mM [70%-^{2}H,^{15}N,^{13}C]-labeled tUIM and non-labeled K63-Ub_2. The intramolecular distance restraints were obtained from 3D ^{15}N- and ^{13}C-edited NOESY spectra with a mixing time of 120 ms and 150 ms, respectively, recorded on 2.4 mM of the [^{15}N,^{13}C]-labeled tUIM and non-labeled K63-Ub_2 complex.

The backbone and side chain chemical shift assignments of K63-Ub_2 were obtained from the following experiments: 2D ^{1}H-^{15}N HSQC, 3D CC(CO)NH, 3D HCC(CO)NH, 2D ^{1}H-^{13}C HSQC, 3D ^{13}C-edited NOESY and 3D ^{15}N-edited NOESY with a mixing time of 120 ms recorded on 1.6 mM [^{13}C,^{15}N]-labeled proximal ubiquitin and non-labeled tUIM or 2.9 mM [^{13}C,^{15}N]-labeled distal ubiquitin and non-labeled tUIM.

The intermolecular distance restraints were obtained from ^{15}N-edited (F2)/^{15}N,^{13}C-filtered (F1) NOESY and ^{13}C-edited (F2)/^{15}N,^{13}C-filtered (F1) NOESY spectra with a mixing time of 250 ms recorded on [^{15}N,^{13}C]-labeled tUIM and a non-labeled K63-Ub_2 complex as well as ^{13}C-edited (F2)/^{15}N,^{13}C-filtered (F1) NOESY spectra with a mixing time of 250 ms recorded on [^{13}C,^{15}N]-labeled proximal ubiquitin or 2.9 mM [^{13}C,^{15}N]-labeled distal ubiquitin and non-labeled tUIM.

The $\{^1H\}$-^{15}N steady-state NOE values were acquired as described (Ikegami et al. 1999) at 310 K on a Bruker Avance II-700 with an ^{15}N frequency of 71.0 MHz. In the $\{^1H\}$-^{15}N steady-state NOEs experiments, relaxation delays of 5 s were applied before saturating the ^1H nucleus for 3 s.

Chemical shift perturbation

Chemical shift perturbations were analyzed by comparing free K63-Ub_2 with the K63-Ub_2 and tUIM complex containing [^{13}C,^{15}N]-labeled proximal ubiquitin or [^{13}C,^{15}N]-labeled distal ubiquitin. Chemical shifts of free K63-Ub_2 were reported by Tenno et al. (Tenno et al. 2004), and those of K63-Ub_2 in complex with the tUIM were obtained from our experiments. Average chemical shift changes of the backbone ^{15}N and ^1H resonances of K63-Ub_2 upon binding to the tUIM were calculated using the following equation: $\Delta\delta = \{\Delta H^2 + (\Delta N/6.51)^2\}^{1/2}$, where ΔH and ΔN represent the changes in chemical shifts of the ^1H and ^{15}N nuclei, respectively.

Paramagnetic relaxation enhancement

Purified tUIM were spin-labeled with MTSL [(1-Oxyl-2, 2, 5, 5-Tetramethyl-Δ^3-Pyrroline-3-Methyl) Methanethiosulfonate]. Spin-labeling reactions were performed in 20 mM potassium phosphate buffer, pH 6.8, 0.5 M NaCl and a 10-fold excess of MTSL, and the reaction solution was incubated at 4°C overnight. Excess MTSL reagent was removed by dialysis into NMR buffer (20 mM potassium phosphate buffer, pH 6.8, and 1 mM DTT) at 4°C. PRE experiments were performed in triplicate.

Residual dipolar coupling

RDC samples were prepared as described (Chou et al. 2001). The K63-Ub_2:tUIM complex with [^{13}C,^{15}N]-labeled proximal or [^{13}C,^{15}N]-labeled distal ubiquitin and the free [^{15}N,^{13}C]-labeled tUIM were soaked in a cylindrically shaped 4% polyacrylamide gel, initially 6 × 9 mm in size, which was subsequently radially compressed to fit within an NMR tube, thereby increasing its length to 18 mm. ^1H-^{15}N residual dipolar couplings were obtained from IPAP-[^1H-^{15}N]-HSQC experiments carried out with ^{13}C decoupling (Wang et al. 1998). The uncertainties in the coupling constant and order parameter for each residue were set to 0.5 Hz and 1.0, respectively. RDC data analysis was performed using PALES (Zweckstetter and Bax 2000) and MODULE 1.0 (Dosset et al. 2001).

Structure calculation of the K63-Ub_2:tUIM complex

We performed automatic structure calculations and NOESY assignments using CYANA version 3.0 (Güntert et al. 1997) and its CANDID algorithm (Herrmann et al. 2002). In the calculations, the program CYANA treated the region comprising residues 1–70 in each ubiquitin as a rigid body by employing new residue types having no torsion angles, which decreased the degree of freedom and improved the efficiency of the torsion angle dynamics. The first conformer of ubiquitin NMR structures (PDB code 1D3Z) was used as a template structure for the new residue. PREDITOR (Berjanskii et al. 2006) (http://wishart.biology.ualberta.ca/shiftor/cgi-bin/preditor_current.py) was used to predict the backbone torsion angles of the tUIM based on the assigned chemical shifts. Backbone hydrogen bond restraints were generated in the secondary structural region and were evaluated by the predicted torsion angles and NOE patterns. The CYANA/CANDID cycles used these two restraints in addition to the NOE-based distance restraints. To aid in the determination of the relative orientations between K63-Ub_2 and the tUIM in the initial stage, we included manually assigned intermolecular NOE restraints only in cycle 1 and 2, but not in the other cycles. We tried several tens of CYANA/CANDID runs until reaching the final result. All the intermolecular NOE assignments were confirmed by manually inspecting the spectra. In the refinement stage, we generated 100 structures that did not show significant violations against the input restraints by CYANA. At this point, in addition to the restraints mentioned, we added residual dipolar coupling data as a restraint with a tolerance of 0.5 Hz. The 100 structures were further minimized by the AMBER software package (Case et al. 2010). Finally, the best 20 structures were selected, and the one that was closest to the mean structure was selected as the representative K63-Ub_2:tUIM complex structure.

ITC measurements

The binding affinities of the tUIM for Ub and K63-Ub_2 were determined by isothermal titration calorimetry (ITC) at 25°C using a MicroCal VP-ITC calorimeter. The protein samples were dialyzed into a buffer containing 20 mM Tris–HCl, pH 7.5, 150 mM NaCl and 5 mM 2-mercaptoethanol and were thoroughly degassed before the titration experiments. Five microliters of approximately 1.3 mM tUIM was injected at 5 min intervals into the 1.4-ml sample cell containing approximately 0.02 mM Ub or K63-Ub_2. The baseline-corrected data were analyzed using software provided by the manufacturer (MicroCal). The first data point was excluded from the analysis, and two independent titration experiments were performed for each interaction. All the data were analyzed using a 1:1 binding model.

The heat capacity between the K63-Ub_2 and the tUIM was determined by MicroCal iTC_{200} calorimetry. The

buffer conditions and concentrations of protein samples were the same as those described above. Three microliters of tUIM were injected at 120 s intervals into the 0.2-ml sample cell containing K63-Ub_2 at 15, 20, 25 and 30°C.

Results

Specific binding of the Rap80 tUIM to K63-linked Ub_2

Rap80 is a 719-amino acid protein that possesses tandem ubiquitin-interacting motifs ($tUIM_{Rap80}$) at its N-terminus; the linker region between two UIMs consists of 10 amino acids. The $tUIM_{Rap80}$ and the linker region are highly conserved in eukaryotes, revealing neither a gap nor an insertion in the sequence alignment (Fig. S1). Particularly, there is little change in the residues that have been identified as essential for binding to ubiquitin in previous structural studies of canonical ubiquitin and UIM complexes (Fisher et al. 2003; Swanson et al. 2003; Wang et al. 2005; Young et al. 1998), which suggests that all of these sequences have similar ubiquitin-binding features. To characterize the interaction between Rap80 and ubiquitin chains in detail, we constructed a polypeptide comprising $tUIM_{Rap80}$ and examined the binding affinity of the $tUIM_{Rap80}$ for monoubiquitin (Ub), Lys48-linked diubiquitin (K48-Ub_2) and Lys63-linked diubiquitin (K63-Ub_2) by isothermal titration calorimetry (ITC). The heat generated during the binding of the $tUIM_{Rap80}$ to Ub and K48-Ub_2 was too small to estimate the affinity in our ITC experiments, most likely indicating a weak interaction. By contrast, the heat generated for the binding of the $tUIM_{Rap80}$ to K63-Ub_2 was much larger, and the thermogram was successfully fit assuming a 1:1 binding model, which yielded dissociation constants, K_d, of 9.1 ± 0.1 μM (Fig. 1). These results indicate that the $tUIM_{Rap80}$ specifically binds to Lys63-linked Ub_2, which is consistent with a previous study that examined this interaction by ITC and fluorescence anisotropy (Sims and Cohen 2009).

Spatial arrangement of the tUIM and ubiquitin subunits

Next, we investigated the relative orientation of the $tUIM_{Rap80}$ bound to K63-Ub_2. Assuming the two UIM motifs serve as interfaces for each ubiquitin subunit, we must consider two possibilities for the binding mode between $tUIM_{Rap80}$ and K63-Ub_2—UIM1:distal, UIM2:proximal, the inverse of these interactions or a mixture of both modes. We therefore examined the binding mode using paramagnetic relaxation enhancement (PRE) measurements. The spin-label MTSL was covalently attached to Cys121 in the C-terminal region of the $tUIM_{Rap80}$ (Fig. 2a), which was in complex with ^{15}N-labeled K63-Ub_2. We produced two labeled K63-Ub_2 samples (^{15}N-labeled distal or ^{15}N-labeled proximal subunit) to selectively observe the PRE effects of spin-labeled $tUIM_{Rap80}$ on NMR signals from the labeled

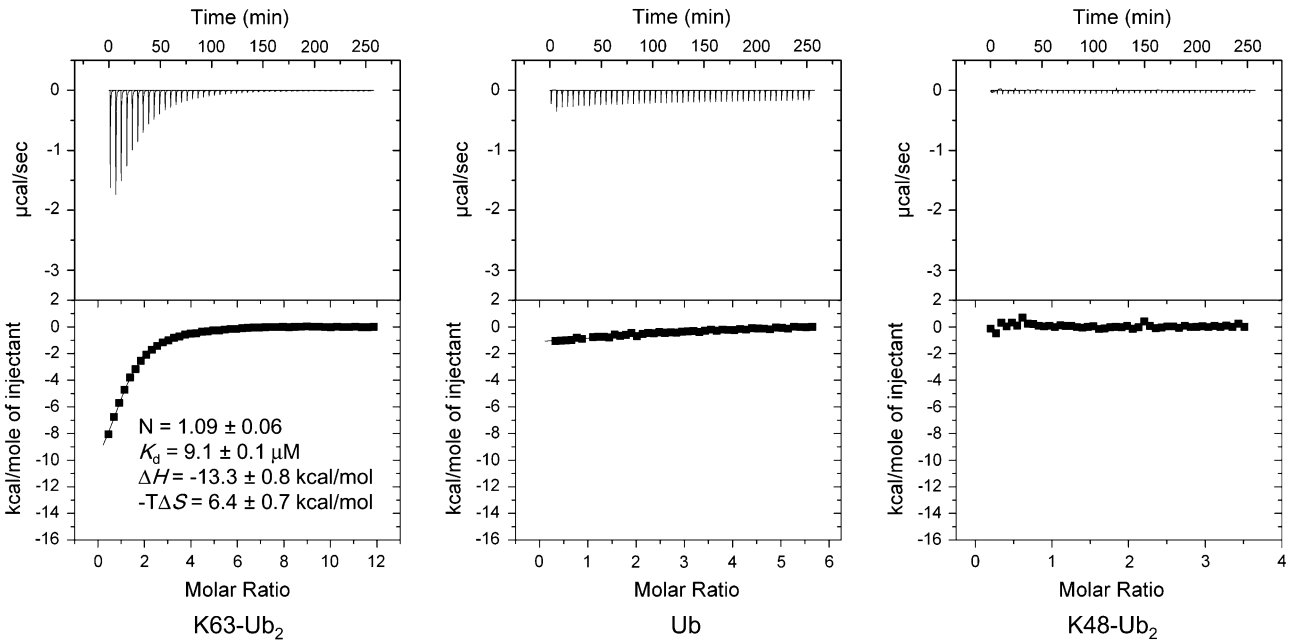

Fig. 1 Calorimetric study of the binding of the $tUIM_{Rap80}$ to K63-Ub_2 or K48-Ub_2. The top panels show ITC thermograms obtained from a titration of K63-Ub_2, Ub or K48-Ub_2 with the $tUIM_{Rap80}$. The bottom panels show the integrated heat per injection after correcting for the heat of dilution of the $tUIM_{Rap80}$. The curve in each bottom panel represents the best fit to a model assuming 1:1 binding (Origin, MicroCal). N, binding stoichiometry; K_d, dissociation constant; ΔH, binding enthalpy; ΔS, binding entropy

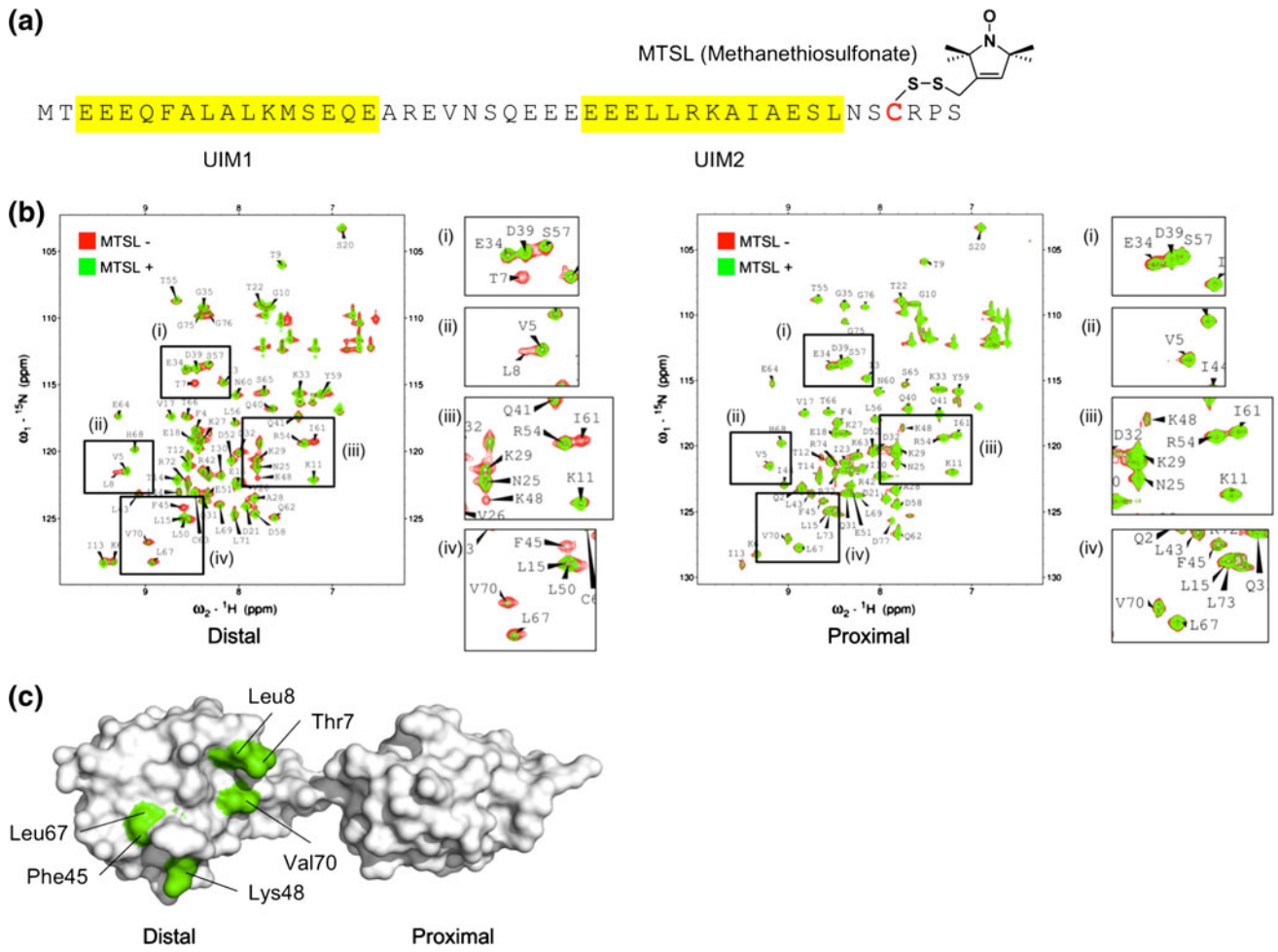

Fig. 2 Relative position of the two UIM motifs in a complex with K63-Ub_2. **a** Amino acid sequence of the $tUIM_{Rap80}$. Residues forming a pair of UIM motifs are highlighted in *yellow*. A paramagnetic spin label, MTSL, is attached via a disulfide bond to Cys121 (colored in *red*) at the C-terminus of the $tUIM_{Rap80}$. **b** Comparison of ^{1}H-^{15}N HSQC spectra of the proximal or distal ubiquitin between MTSL-labeled (*green*) and non-labeled (*red*) $tUIM_{Rap80}$. Spectra of the proximal or distal ubiquitin in the selected areas are magnified. The signals of Thr7 and Leu8 in the proximal ubiquitin are missing. **c** Paramagnetic relaxation enhancement of K63-Ub_2 bound to spin labeled $tUIM_{Rap80}$. The residues whose signals were attenuated upon complex formation are shown in *green*, indicating a paramagnetic relaxation enhancement effect on the distal ubiquitin in K63-Ub_2

subunit. The amide ^{1}H-^{15}N cross-peaks of Thr7, Leu8, Phe45, Lys48, Ile61 and Val70 from the K63-Ub_2 distal subunit completely disappeared, in addition to partial attenuation of Leu67 (Fig. 2b, c), whereas essentially no change was observed in the cross-peaks from the proximal subunit (Fig. 2b). These results unambiguously indicate that the C-terminal motif of the $tUIM_{Rap80}$, $UIM2_{Rap80}$, specifically binds to the distal subunit. In Fig. 2c, the residues that experience attenuation by PRE are mapped onto the structure of K63-Ub_2. They show a discontinuous pattern, in which one can recognize two separated regions affected by the spin label. One comprises Thr7, Leu8 and Val70 and the other comprises Phe45, Lys48 and Leu67. In each region, affected residues create somewhat a continuous surface, although data could not obtain for Ala46 and Gly47, which locate between Phe45 and Lys48. The PRE blank section between these two surfaces is bound and covered by $UIM2_{Rap80}$ in the complex structure (Fig. 5). Thus, the spin-label would not be able to access the section, making the discontinuous PRE pattern. Given the 1:1 stoichiometry of the complex in the ITC measurements, the N-terminal motif of the $tUIM_{Rap80}$, $UIM1_{Rap80}$, is likely to bind to the proximal subunit in agreement with the crystal structure of the tUIM of mouse Rap80 in complex with K63-Ub_2 (Sato et al. 2009a).

We next asked whether the position of the two ubiquitin subunits was fixed in the $tUIM_{Rap80}$ complex in solution. To answer this question, we measured ^{1}H-^{15}N RDC values for the proximal and distal ubiquitin subunits in the complex using a pair of reciprocally ^{15}N-labeled K63-Ub_2 samples. The RDC data for proximal and distal ubiquitin were both in excellent agreement with the monoubiquitin structure (PDB

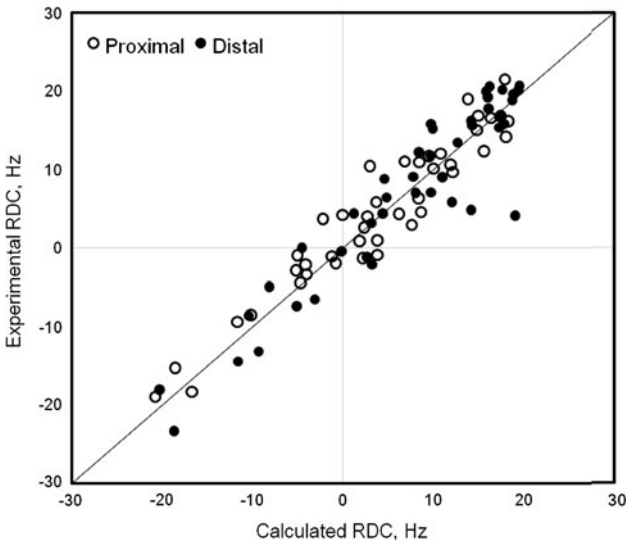

Fig. 3 Relative orientation of the proximal and distal subunits of K63-Ub_2 bound to the $tUIM_{Rap80}$. Comparison of the ^{1}H-^{15}N residual dipolar coupling constants between the proximal (*open circles*) and distal ubiquitin (*filled circles*) in the K63-Ub_2:$tUIM_{Rap80}$ complex. The calculated values were estimated from the monoubiquitin structure (PDB code 1D3Z). The *vertical* and *horizontal axes* represent the calculated and experimental values for each residue, respectively

code 1D3Z) (correlation coefficient r = 0.937 for proximal Ub and 0.936 for distal Ub) (Fig. 3). This result demonstrates that each ubiquitin subunit in the complex retains the structure of monoubiquitin. The axial components of two ubiquitin subunits were lined up in the same direction estimated by the RDC data. Considering the isopeptide linkage between K63 of the proximal ubiquitin and the carboxyl terminus of the distal ubiquitin, the two ubiquitin subunits were linearly aligned in the complex for spatial restriction.

To evaluate structural differences between the solution and crystal forms of K63-Ub_2 in the complex, the experimental RDC data were compared with those calculated from the crystal structures of free K63-Ub_2 (PDB code 2JF5) and the mouse Rap80 tUIM:K63-Ub_2 complex (PDB code 3A1Q). Although the two ubiquitin subunits adopt an extended configuration in both crystal structures, superposition of their proximal subunits showed that the proximal subunits were rotated 180° in relation to each other (Komander et al. 2009; Sato et al. 2009a). The experimental data exhibited better agreement with the K63-Ub_2 structure in the Rap80-bound form (r = 0.879) than in the free form (r = 0.816). Considering the orientational degeneracy in RDC analysis, which allows for 180° rotations about the axis of the alignment tensor, the relative orientation of the two ubiquitin subunits cannot be directly defined. However, these results suggest that, in solution, two ubiquitin subunits bound to $tUIM_{Rap80}$ are aligned in a similar manner to the K63-Ub2 bound to mouse Rap80 tUIIMs in the crystal structure.

Solution structure of the K63-Ub_2:tUIM complex

To obtain more detailed structural information, we performed structure calculations of the complex based on NMR data. It should be noted that this complex has three structural domains, the $tUIM_{Rap80}$, and the proximal and distal ubiquitin subunits, and thus is expected to have a non-globular shape. Furthermore, inter-subunit NOE restraints between two Ub units would be sparse because there are few direct contacts, making the determination of the solution structure difficult.

Using CYANA/CANDID, we calculated the $tUIM_{Rap80}$ structure in the complex while simultaneously optimizing the intermolecular positions. The excellent agreement of the RDC data with monoubiquitin allowed us to assume each ubiquitin subunit was a rigid body. The core part (residues 1–70) of each ubiquitin was treated as a rigid body in the calculation, increasing the efficiency of the torsion angle dynamics simulation. Intermolecular restraints were obtained from isotope-edited and filtered NOESY experiments (Fig. 4). A total of 555 NMR-derived distance restraints, including 47 intermolecular restraints and 85 torsion angle restraints, were obtained and used for the final calculation with 84 RDC restraints (Table 1). Among 89 conformers that did not show significant violations after the AMBER refinement, a group of 52 conformers with lower intra-molecular van der Waals energies of the $tUIM_{Rap80}$ region than the others was selected (Fig. S2). Finally, the 20 lowest-energy structures were selected from the group as a final ensemble and subjected to further analyses.

The final 20 structures were well converged (Fig. 5a); the RMSD values of the backbone and all heavy atoms over residues 1–70 of the proximal and distal ubiquitins and residues 81–120 of $tUIM_{Rap80}$ were 0.46 ± 0.30 and 0.64 ± 0.27 Å, respectively. The structures showed reasonable geometry, with 95.4% of the residues in the most favorable regions, 3.8% in the additional allowed regions and 0.8% in the generously allowed regions of the Ramachandran plot, as defined by the program PROCHECK (Laskowski et al. 1993). We compared these structures with the structures calculated without the RDC data; Monte Carlo simulations of the RDC data fitting showed better agreement with the structures with RDC data than those without RDC data (r = 0.931 ± 0.002 and 0.831 ± 0.010, respectively), which suggests the central role of RDC restraints in determining the relative orientation. The deviation of the magnitude of the obtained axial and rhombic components of the alignment tensor, Da and Dr,

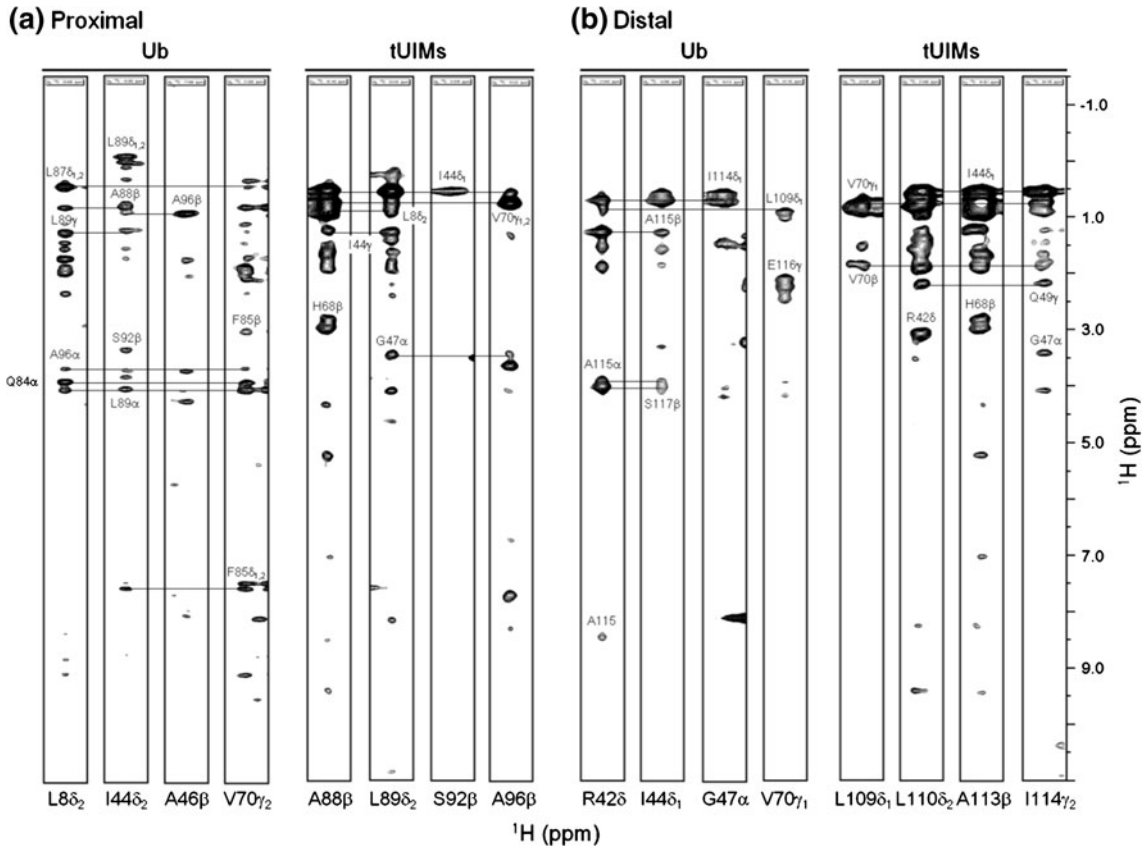

Fig. 4 Intermolecular NOEs in the K63-Ub_2:$tUIM_{Rap80}$ complex. Strips selected from three-dimensional ^{13}C-edited (F2)/^{15}N, ^{13}C-filtered (F1) NOESY spectra depict intermolecular NOEs between the proximal ubiquitin and the $tUIM_{Rap80}$ (**a**) and between the distal ubiquitin and the $tUIM_{Rap80}$ (**b**)

Table 1 NOE restraints and NMR structure statistics

NOE restraints	
Total	508
Intra	113
Sequential ($\|i–j\| = 1$)	162
Medium-range ($2 \leq \|i–j\| \leq 4$)	231
Long-range ($\|i–j\| \geq 5$)	2
Intermolecular	47
Distal:tUIM	15
Proximal:tUIM	32
Hydrogen bonds	33
Torsion angle restraints for tUIM (ϕ/ψ)	43/42
Final statistics of 20 structures	
AMBER energy (kcal/mol)	$-4{,}745 \pm 86$
Constraint energy (kcal/mol)	7 ± 3
Maximum violations	
Distance (Å)	0.202
Angle (°)	1.428
Mean deviations from ideal geometry	
Bond lengths (Å)	0.0103 ± 0.0001
Bond angles (°)	1.92 ± 0.01

were small ($Da = -10.117 \pm 0.156$ and $Dr = 0.531 \pm 0.019$).

The NMR structure of the $tUIM_{Rap80}$ superimposed onto the crystal structure of the mouse Rap80 tUIM (PDB code 3A1Q, chain F) with an RMSD of 2.9 Å over 40 Cα atoms. Our structure shows that the $tUIM_{Rap80}$ forms an α-helix and that the proximal and distal subunits of the K63-Ub_2 bind to $UIM1_{Rap80}$ and $UIM2_{Rap80}$, respectively. The linker region between $UIM1_{Rap80}$ and $UIM2_{Rap80}$ also formed an α-helix, which is consistent with the crystal structure. However, the relative orientation of the two ubiquitin subunits in solution differs slightly from that in the crystal, which is represented by a structure comparison (Fig. S3).

The interaction was formed via a hydrophobic surface composed of Ile44-centered residues of each ubiquitin subunit with hydrophobic residues and a serine residue of each UIM that line up at the same side of the $tUIM_{Rap80}$ (Fig. 5b). The contact between the proximal subunit and $UIM1_{Rap80}$ buried a total of 531 $Å^2$ while that between the distal subunit and $UIM2_{Rap80}$ buried a total of 400 $Å^2$ of surface area. The interaction surface was consistent with the chemical shift perturbation (CSP) of K63-Ub_2 upon binding to the $tUIM_{Rap80}$. The CSP mapped onto the

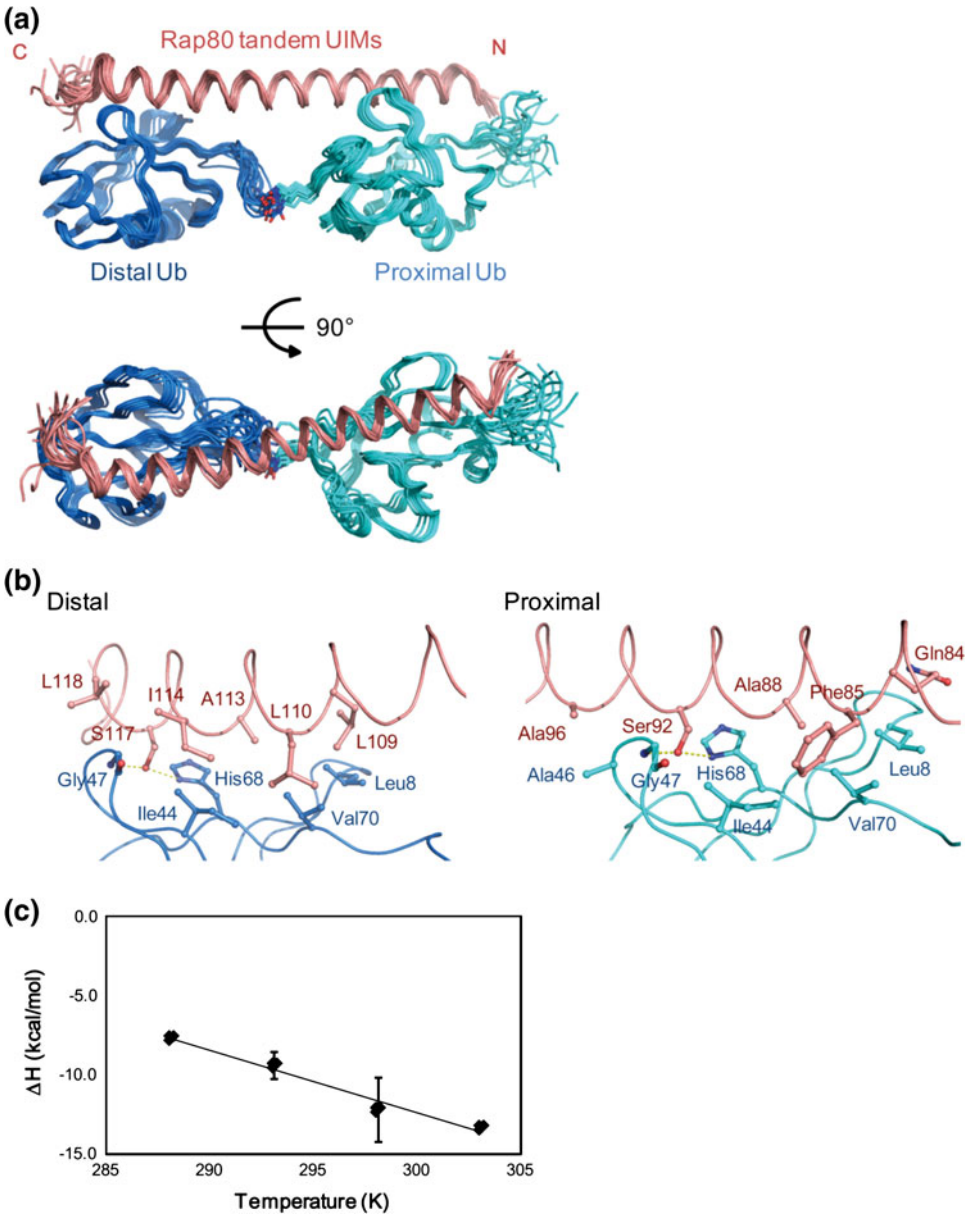

Fig. 5 Solution structure of the K63-Ub_2:$tUIM_{Rap80}$ complex. **a** An overview of the superimposed Cα traces of the final 20 NMR structures of the K63-Ub_2:$tUIM_{Rap80}$ complex. The distal and proximal ubiquitin subunits of K63-Ub_2 are shown in blue and cyan, respectively. The $tUIM_{Rap80}$ are shown in pink. **b** Close-up views of the interfaces between K63-Ub_2 and $tUIM_{Rap80}$. The $tUIM_{Rap80}$ interaction surfaces of the distal and proximal subunits are shown in the *left* and *right panels*, respectively. The side chains responsible for the interaction are indicated as *stick models*. *Broken lines* indicate potential hydrogen bonds (< 3.3 Å). **c** The heat capacity change ΔC_p for the K63-Ub_2:$tUIM_{Rap80}$ complex formation. The value of ΔC_p (−397 cal/mol K) was determined by measuring the temperature dependence of the ΔH parameter at 15, 20, 25 and 30°C

ubiquitin structure (PDB code 1D3Z) revealed that the $tUIM_{Rap80}$ bound to a β-sheet patch on the distal or proximal ubiquitin (Fig. S4). The NMR structure showed that the $tUIM_{Rap80}$ bound to the hydrophobic patch of ubiquitin in a manner similar to other consensus UIMs. Conserved hydrophobic residues in $UIM1_{Rap80}$, Phe85, Ala88, Leu89 and Ala96, interact with the hydrophobic surface of the proximal subunit composed of Leu8, Ile44, Ala46 and Val70. Hydrophobic residues of $UIM2_{Rap80}$, Leu109, Ala113, Ile114 and Leu118, interact with the hydrophobic surface of the distal subunit composed of Leu8, Ile44 and Val70. In addition, Ser92 Oδ of $UIM1_{Rap80}$ makes hydrogen bonds with Gly47 N and His68 Nδ1 of the proximal subunit. Glu95 Oε of $UIM1_{Rap80}$ also forms a hydrogen bond with Thr66 Oγ1 of the proximal subunit. Hydrogen bonds are also found between Ser117 Oδ of $UIM2_{Rap80}$ and Gly47 N and His68 Nδ1 of the distal subunit (Fig. 5b).

Thus, the K63-Ub_2:$tUIM_{Rap80}$ complex formation involves the burial of solvent-exposed surfaces, which can cause large changes in thermodynamic parameters. To reveal the thermodynamic character of complex formation between K63-Ub_2 and $tUIM_{Rap80}$, we measured the temperature dependence of the enthalpy change, ΔH, associated with the interaction at 15, 20, 25 and 30°C by ITC to obtain the heat capacity at constant pressure, ΔC_p (Fig. 5c). The experimental ΔC_p was −397 cal/mol K, and the estimated ΔC_p based on the buried interfacial area of the complex structure was −336 cal/mol K (Nozaki and Tanford 1971), which is in good agreement with the experimental value.

Conformational change of tUIM upon complex formation

The solution structure of the K63-Ub_2:$tUIM_{Rap80}$ complex showed that the linker region (residues 96–105) between $UIM1_{Rap80}$ and $UIM2_{Rap80}$ forms an α-helix, representing a stable conformation as in the crystal structure. Next, we investigated the $tUIM_{Rap80}$ structure in a free state in solution.

To obtain structural information on free $tUIM_{Rap80}$, we predicted the secondary structure based on the $^{13}C\alpha$ chemical shift (Fig. 6a) (Wishart et al. 1991). In the free form, the regions of $UIM1_{Rap80}$ and $UIM2_{Rap80}$ showed a moderate downfield shift, which is typical for helical structure, whereas the linker region was predicted to adopt a random-coil. Complex formation induced larger downfield shifts in most of the $tUIM_{Rap80}$ residues, especially in the linker region, residues 94–107, and the very C-terminal region of UIM2, residues 118–124. This result showed that complex formation enhanced the propensity of α-helicity of the linker, which aligns two UIM helices in one long helix. This increase in structure was further supported by the $\{^1H\}$-^{15}N steady-state NOE values of the linker, which were significantly lower than those for the UIM regions in the free form whereas the values for both regions were similar in the complex form (Fig. 6b).

Residues 97 to 102 of the $tUIM_{Rap80}$ do not adopt an α-helix in the free form as the RDC values in the region substantially deviate from those calculated from the complex form of the $tUIM_{Rap80}$ (Fig. 6c). The alignment tensors of UIM1 (residues 82–96) and UIM2 (residues 109–118) obtained with Module (Dosset et al. 2001) suggest that the two UIM helices are parallel to each other. Nevertheless, because of the flexibility of the linker region, they do not have to be collinear in the free form.

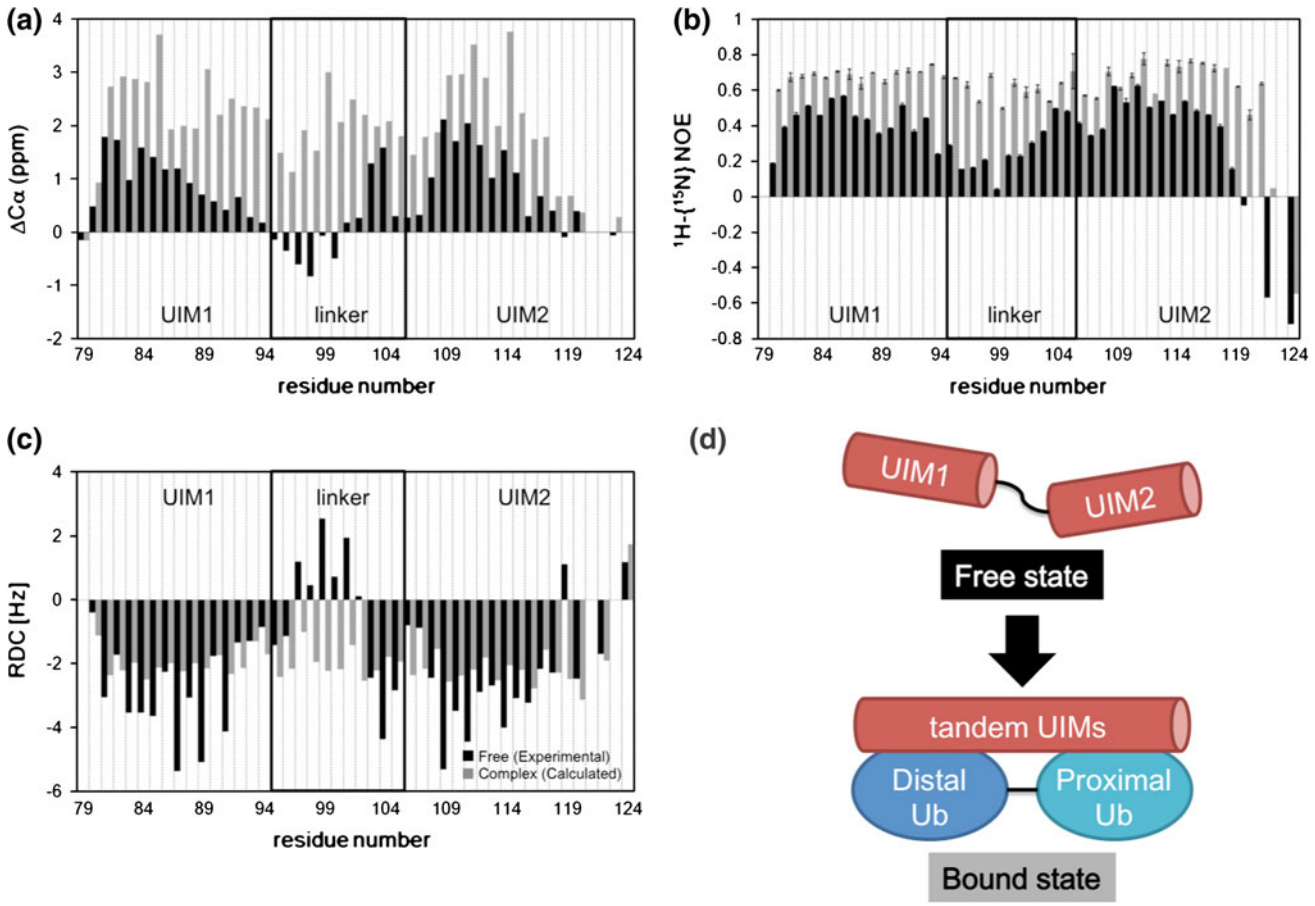

Fig. 6 A random-coil to helix transition of the $tUIM_{Rap80}$ linker region upon binding to K63-Ub_2. Comparison of NMR parameters of the $tUIM_{Rap80}$ between the free (*black bars*) and the K63-Ub_2-bound (*gray bars*) forms; **a** chemical shifts of Cα; **b** $\{^1H\}$-^{15}N steady-state NOE values; **c** RDC values of free $tUIM_{Rap80}$ (*black*) obtained experimentally and RDC values of the $tUIM_{Rap80}$ calculated from the K63-Ub_2-bound $tUIM_{Rap80}$ structure (*gray*). These data show that the linker between UIM1 and UIM2 is non-helical and mobile in the free form. This property is distinct from the two UIM motifs, which exhibit a helical propensity even in the free state. **d** Model of the K63-Ub_2:$tUIM_{Rap80}$ complex formation associated with conformational changes. Pairs of structural motifs in K63-Ub_2 and the $tUIM_{Rap80}$ are separated by a flexible linker in a free state. Complex formation induces the rigid conformation involved in a random-coil to helix transition in the $tUIM_{Rap80}$

Discussion

Structure and the interaction of the complex

Although the structure of the $tUIM_{Rap80}$:K63-Ub_2 complex was previously solved by X-ray crystallography (Sato et al. 2009a), substantial flexibility of $tUIM_{Rap80}$ and K63-Ub_2 in the free state has raised the question of whether the stable structure observed in the crystal is maintained in solution. To address this issue, we employed solution NMR and determined the complex structure between $tUIM_{Rap80}$ and K63-Ub_2 based on RDC and NOE-derived restraints. The structure revealed that the two ubiquitin subunits of K63-Ub_2 are in an extended configuration and that bound $tUIM_{Rap80}$ adopts a long continuous α-helix. The overall structure of the K63-Ub_2:$tUIM_{Rap80}$ complex in solution is very similar to that in the crystal structure (Sato et al. 2009a), with a common interaction mode for each Ub:UIM pair. The relative angle and distance between the two ubiquitin subunits differed slightly from those of the mean NMR structure (the angle is 3.0° smaller, and the distance is 0.2 Å longer than those in the crystal). However, the difference is within the deviation present among the calculated NMR structures (backbone RMSD 0.46 ± 0.30 Å), indicating that the crystal structure is essentially maintained in solution. The residues affected in the PRE experiments are located exclusively on one side of the distal Ub and were absent in the proximal Ub. This observation demonstrates that there is no other significant binding mode.

Helix formation of the inter UIM linker

The helix formation of the linker region, which is the critical step for the $tUIM_{Rap80}$ to form a continuous helix, is likely to be context-dependent; the relative positions of the two UIM helices with a fixed distance imposed in the complex might promote the linker region to form a helix (Fig. 6d). The result of the transition from a random-coil to a helix in the linker region and the C-terminal region of UIM2 is consistent with previous observations by CD spectroscopy (Sims and Cohen 2009), which showed a gain of helical content upon complex formation. It is assumed that the continuous α-helix of the linker in the $tUIM_{Rap80}$ is crucial for binding to the Lys63-linked polyUb because the selective binding of the $tUIM_{Rap80}$ is influenced by the length of the $tUIM_{Rap80}$ linker region (Sato et al. 2009a). This assumption explains the inability of $tUIM_{Rap80}$ to bind to Lys48-linked polyUb. Due to the large difference in the spatial positions between Lys48- and Lys63-linked polyUb, Lys48-linked polyUb cannot adopt the conformation of K63-Ub_2 in the complex. Despite the structural similarity between K63-Ub_2 and linear-Ub_2 (Komander et al. 2009), the $tUIM_{Rap80}$ showed a lower affinity for linear polyUb than for K63-linked polyUb, as demonstrated by GST-pull down assay (Sato et al. 2009a) and NMR titration (Markin et al. 2010). The low-affinity of $tUIM_{Rap80}$ for linear-Ub_2 was explained by the "molecular ruler" function of $tUIM_{Rap80}$ that precisely determines the relative position of two ubiquitin subunits, discriminating subtle difference between Lys63-linked and linear-linked polyubiquitin chains (Sato et al. 2009a). Interestingly, the ruler, $tUIM_{Rap80}$, is highly flexible in the free state (Markin et al. 2010), although helical propensity is somewhat retained in the UIM regions (Fig. 6). However, the $tUIM_{Rap80}$ helix formed upon complex formation was demonstrated to acquire substantial rigidity, which may contribute to the "molecular ruler" function, because the ruler must have substantial rigidity to precisely discriminate between sub-nanometer distances.

Here, we reported the structural properties of the K63-Ub_2 and human Rap80 tUIM complex examined by various NMR analyses and determined the K63-Ub_2:$tUIM_{Rap80}$ complex structure by NOE- and RDC-based restraints, revealing that the structure of the complex in the crystal is essentially maintained in solution. Together with NMR analyses of free $tUIM_{Rap80}$, the study also showed that the linker region of the $tUIM_{Rap80}$ undergoes a transition from a random-coil to an α-helix upon complex formation with K63-Ub_2, which simultaneously fixes the relative position of ubiquitin subunits.

Acknowledgments We thank Dr. Akio Ojida and Dr. Itaru Hamachi for their help in collecting the ITC data, the NMR Facility of the Yokohama Institute at RIKEN and the High-field Biomacromolecular NMR Core Facility, National Research Program for Genomic Medicine, Taiwan, Republic of China, for collecting the NMR data. This work was supported by grants to M.S. and H.T. from the Ministry of Education, Culture, Sports, Science and Technology (MEXT) of Japan and the Japan Science and Technology Agency. This research was also supported in part by the Global COE Program "International Center for Integrated Research and Advanced Education in Materials Science" (No. B-09) of MEXT of Japan, administered by the Japan Society for the Promotion of Science.

References

Berjanskii M, Neal S, Wishart D (2006) PREDITOR: a web server for predicting protein torsion angle restraints. Nucleic Acids Res 34:W63–W69

Case DA, Darden TA, Cheatham TE III, Simmerling CL, Wang J, Duke RE, Luo R, Walker RC, Zhang W, Merz KM, Roberts BP, Wang B, Hayik S, Roitberg A, Seabra G, Kolossváry I, Wong KF, Paesani F, Vanicek J, Liu J, Wu X, Brozell SR, Steinbrecher T, Gohlke H, Cai Q, Ye X, Wang J, Hsieh M-J, Cui G, Roe DR, Mathews DH, Seetin MG, Sagui C, Babin V, Luchko T, Gusarov S, Kovalenko A, Kollman PA (2010) AMBER 11. University of California, San Francisco

Chou J, Gaemers S, Howder B, Louis J, Bax A (2001) A simple apparatus for generating stretched polyacrylamide gels, yielding uniform alignment of proteins and detergent micelles. J Biomol NMR 21:377–382

Delaglio F, Grzesiek S, Vuister G, Zhu G, Pfeifer J, Bax A (1995) NMRPipe: a multidimensional spectral processing system based on UNIX pipes. J Biomol NMR 6:277–293

Diercks T, Cole M, Kessler H (1999) An efficient strategy for assignment of cross-peaks in 3D heteronuclear NOESY experiments. J Biomol NMR 15:177–180

Dosset P, Hus J, Marion D, Blackledge M (2001) A novel interactive tool for rigid-body modeling of multi-domain macromolecules using residual dipolar couplings. J Biomol NMR 20:223–231

Eddins M, Varadan R, Fushman D, Pickart C, Wolberger C (2007) Crystal structure and solution NMR studies of Lys48-linked tetraubiquitin at neutral pH. J Mol Biol 367:204–211

Fisher R, Wang B, Alam S, Higginson D, Robinson H, Sundquist W, Hill C (2003) Structure and ubiquitin binding of the ubiquitin-interacting motif. J Biol Chem 278:28976–28984

Goddard TD, Kneller DG. SPARKY 3. University of California, San Francisco

Güntert P, Mumenthaler C, Wüthrich K (1997) Torsion angle dynamics for NMR structure calculation with the new program DYANA. J Mol Biol 273:283–298

Herrmann T, Güntert P, Wüthrich K (2002) Protein NMR structure determination with automated NOE assignment using the new software CANDID and the torsion angle dynamics algorithm DYANA. J Mol Biol 319:209–227

Hershko A, Ciechanover A (1998) The ubiquitin system. Annu Rev Biochem 67:425–479

Hicke L (2001) Protein regulation by monoubiquitin. Natl Rev Mol Cell Biol 2:195–201

Hicke L, Schubert H, Hill C (2005) Ubiquitin-binding domains. Natl Rev Mol Cell Biol 6:610–621

Ikeda F, Dikic I (2008) Atypical ubiquitin chains: new molecular signals. 'Protein modifications: beyond review series the usual suspects'. EMBO Rep 9:536–542

Ikegami T, Kuraoka I, Saijo M, Kodo N, Kyogoku Y, Morikawa K, Tanaka K, Shirakawa M (1999) Resonance assignments, solution structure, and backbone dynamics of the DNA- and RPA-binding domain of human repair factor XPA. J Biochem 125:495–506

Ito T, Wagner G (2004) Using codon optimization, chaperone co-expression, and rational mutagenesis for production and NMR assignments of human eIF2 alpha. J Biomol NMR 28:357–367

Kim H, Chen J, Yu X (2007) Ubiquitin-binding protein RAP80 mediates BRCA1-dependent DNA damage response. Science 316:1202–1205

Komander D, Reyes-Turcu F, Licchesi J, Odenwaelder P, Wilkinson K, Barford D (2009) Molecular discrimination of structurally equivalent Lys 63-linked and linear polyubiquitin chains. EMBO Rep 10:466–473

Kulathu Y, Akutsu M, Bremm A, Hofmann K, Komander D (2009) Two-sided ubiquitin binding explains specificity of the TAB 2 NZF domain. Nat Struct Mol Biol 16:1328–1330

Laskowski R, Macarthur M, Moss D, Thornton J (1993) PROCHECK - A program to check the stereochemical qualith of protein structures. J Appl Cryst 26:283–291

Markin C, Xiao W, Spyracopoulos L (2010) Mechanism for recognition of polyubiquitin chains: balancing affinity through interplay between multivalent binding and dynamics. J Am Chem Soc 132:11247–11258

Newton K, Matsumoto M, Wertz I, Kirkpatrick D, Lill J, Tan J, Dugger D, Gordon N, Sidhu S, Fellouse F, Komuves L, French D, Ferrando R, Lam C, Compaan D, Yu C, Bosanac I, Hymowitz S, Kelley R, Dixit V (2008) Ubiquitin chain editing revealed by polyubiquitin linkage-specific antibodies. Cell 134:668–678

Nozaki Y, Tanford C (1971) The solubility of amino acids and two glycine peptides in aqueous ethanol and dioxane solutions. Establishment of a hydrophobicity scale. J Biol Chem 246: 2211–2217

Pickart C, Fushman D (2004) Polyubiquitin chains: polymeric protein signals. Curr Opin Chem Biol 8:610–616

Rahighi S, Ikeda F, Kawasaki M, Akutsu M, Suzuki N, Kato R, Kensche T, Uejima T, Bloor S, Komander D, Randow F, Wakatsuki S, Dikic I (2009) Specific recognition of linear ubiquitin chains by NEMO is important for NF-kappaB activation. Cell 136:1098–1109

Sato Y, Yoshikawa A, Yamagata A, Mimura H, Yamashita M, Ookata K, Nureki O, Iwai K, Komada M, Fukai S (2008) Structural basis for specific cleavage of Lys 63-linked polyubiquitin chains. Nature 455:358–362

Sato Y, Yoshikawa A, Mimura H, Yamashita M, Yamagata A, Fukai S (2009a) Structural basis for specific recognition of Lys 63-linked polyubiquitin chains by tandem UIMs of RAP80. EMBO J 28:2461–2468

Sato Y, Yoshikawa A, Yamashita M, Yamagata A, Fukai S (2009b) Structural basis for specific recognition of Lys 63-linked polyubiquitin chains by NZF domains of TAB 2 and TAB 3. EMBO J 28:3903–3909

Sims J, Cohen R (2009) Linkage-specific avidity defines the lysine 63-linked polyubiquitin-binding preference of rap80. Mol Cell 33:775–783

Sobhian B, Shao G, Lilli D, Culhane A, Moreau L, Xia B, Livingston D, Greenberg R (2007) RAP80 targets BRCA1 to specific ubiquitin structures at DNA damage sites. Science 316:1198–1202

Swanson K, Kang R, Stamenova S, Hicke L, Radhakrishnan I (2003) Solution structure of Vps27 UIM-ubiquitin complex important for endosomal sorting and receptor downregulation. EMBO J 22:4597–4606

Tenno T, Fujiwara K, Tochio H, Iwai K, Morita E, Hayashi H, Murata S, Hiroaki H, Sato M, Tanaka K, Shirakawa M (2004) Structural basis for distinct roles of Lys63- and Lys48-linked polyubiquitin chains. Genes Cells 9:865–875

Varadan R, Assfalg M, Haririnia A, Raasi S, Pickart C, Fushman D (2004) Solution conformation of Lys63-linked di-ubiquitin chain provides clues to functional diversity of polyubiquitin signaling. J Biol Chem 279:7055–7063

Wang Y-X, Marquardt JL, Wingfield P, Stahl SJ, Lee-Huang S, Torchia D, Bax A (1998) Simultaneous measurement of 1H–15 N, 1H–13C', and 15 N − 13C'dipolar couplings in a perdeuterated 30 kDa protein dissolved in a dilute liquid crystalline phase. J Am Chem Soc 120:7385–7386

Wang Q, Goh A, Howley P, Walters K (2003) Ubiquitin recognition by the DNA repair protein hHR23a. Biochemistry 42: 13529–13535

Wang Q, Young P, Walters K (2005) Structure of S5a bound to monoubiquitin provides a model for polyubiquitin recognition. J Mol Biol 348:727–739

Wishart D, Sykes B, Richards F (1991) Relationship between nuclear magnetic resonance chemical shift and protein secondary structure. J Mol Biol 222:311–333

Young P, Deveraux Q, Beal R, Pickart C, Rechsteiner M (1998) Characterization of two polyubiquitin binding sites in the 26 S protease subunit 5a. J Biol Chem 273:5461–5467

Zhang N, Wang Q, Ehlinger A, Randles L, Lary J, Kang Y, Haririnia A, Storaska A, Cole J, Fushman D, Walters K (2009) Structure of the s5a:k48-linked diubiquitin complex and its interactions with rpn13. Mol Cell 35:280–290

Zweckstetter M, Bax A (2000) Prediction of sterically induced alignment in a dilute liquid crystalline phase: Aid to protein structure determination by NMR. J Am Chem Soc 122:3791–3792